ACS Biomaterials SCIENCE & ENGINEERING

pubs.acs.org/journal/abseba

Article

Genetically Encoded Interpenetrating Polymer Networks as Injectable Biomaterials for Controlled Therapeutic Protein Delivery

Murial L. Ross, Shivani P. Kottantharayil, Tina K. Nguyen, Rashmi Ravichandran, and Cole A. DeForest*

Cite This: *ACS Biomater. Sci. Eng.* 2025, 11, 4869−4880

Read Online

ACCESS | Metrics & More | Article Recommendations | Supporting Information

ABSTRACT: Though recombinant protein therapeutics hold great potential in treating many diseases, their intravenous delivery introduces challenges with off-target effects and short circulation half-lives. Injectable biomaterial depots have proven useful in confining therapeutic administration to specific bodily locations but have faced difficulties in simultaneously controlling drug release, network mechanics, and functionalization. Toward addressing these limitations, this work introduces the first recombinant protein-based interpenetrating polymer network (IPN), which we exploit for injectable therapeutic deposition. Each of the self-sorting telechelic biopolymer networks is comprised of an intrinsically disordered XTEN protein midblock differentially flanked with one of two orthogonally self-assembling coil domains that enable rapid shear-thinning and self-healing responsiveness in biomaterials with tunable viscoelasticity. Exploiting the orthogonal and genetically encoded click-like SpyLigation/SnoopLigation chemistries to independently tether proteins-of-interest to each underlying network, we demonstrate that fluorescent proteins and growth factors (rhIGF-1, rhEGF) can be released in a controlled fashion from materials with tunable viscoelasticity while retaining high bioactivity following network dissolution. Such recombinant IPN biomaterials offer exciting opportunities for next-generation biotherapeutic delivery.

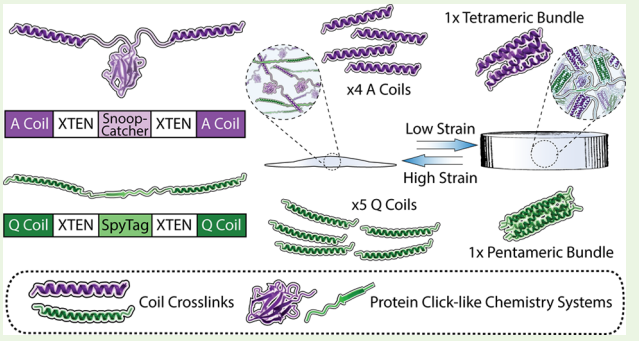

KEYWORDS: *biomaterials, drug delivery, recombinant proteins, coiled-coils, injectable*

INTRODUCTION

Owing to their promising specificity and efficacy compared to standard small molecules, recombinant proteins have become an increasingly popular type of therapeutic drug.[1] These therapeutics have been designed to treat a wide variety of ailments (e.g., cancer, cardiac/vascular disease, blood disorders, autoimmunity, many infectious diseases[2]) and encompass the majority of functional protein classes (e.g., monoclonal antibodies, coagulation factors, replacement enzymes, growth factors[2]). Recombinant growth factors and other protein therapeutics are often delivered via intravenous injection, as well as topically or intralesionally.[3−5] Unfortunately, the efficacy of such drug delivery strategies is impeded by short half-lives in circulation/tissue due to low protein stability, proteolytic degradation, and rapid clearance, necessitating multiple injections per week to achieve clinical outcomes.[4,6−9] Additionally, intravenous injection often leads to off-target accumulation, decreasing the amount of therapeutically available drug while increasing the risk of deleterious side effects.[4,7−10] As such, there is a dire need to engineer tunable delivery systems that offer extended presentation and local efficacy of therapeutic proteins.

One particularly exciting direction for controlled drug delivery involves the use of injectable biomaterials that can serve as therapeutic depots. Hydrogels—water-swollen polymeric networks—are a useful class of biomaterials for therapeutic delivery due to their ability to elute drugs in a controlled and tunable manner.[4,7,10−12] Recent and exciting work has sought to design novel recombinant protein-based hydrogels for drug delivery,[13−19] including by utilizing coiled-coil fibrous hydrogels to encapsulate hydrophobic small molecules[20] or covalently ligated networks via protein click-like chemistries systems to release mock protein drugs.[21] Prime biomaterial candidates for therapeutic delivery offer (1) well-defined mechanics, readily tailored to a specific application,[10,22] (2) injectability, permitting localized drug release in a minimally invasive manner that minimizes systemic side effects,[5,6,8,23,24] (3) functionalizability, such that varying amounts of therapeutic cargos can be coformulated for extended release,[5,6,8] (4) multiplexability, able to deliver multiple protein drugs for a sustained period of time,[3,6,9] (5) chemically defined species, enabling enhanced property control and decreased batch-to-

Received: April 25, 2025
Revised: June 17, 2025
Accepted: June 20, 2025
Published: July 3, 2025

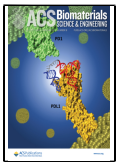

https://doi.org/10.1021/acsbiomaterials.5c00813
ACS Biomater. Sci. Eng. 2025, 11, 4869−4880

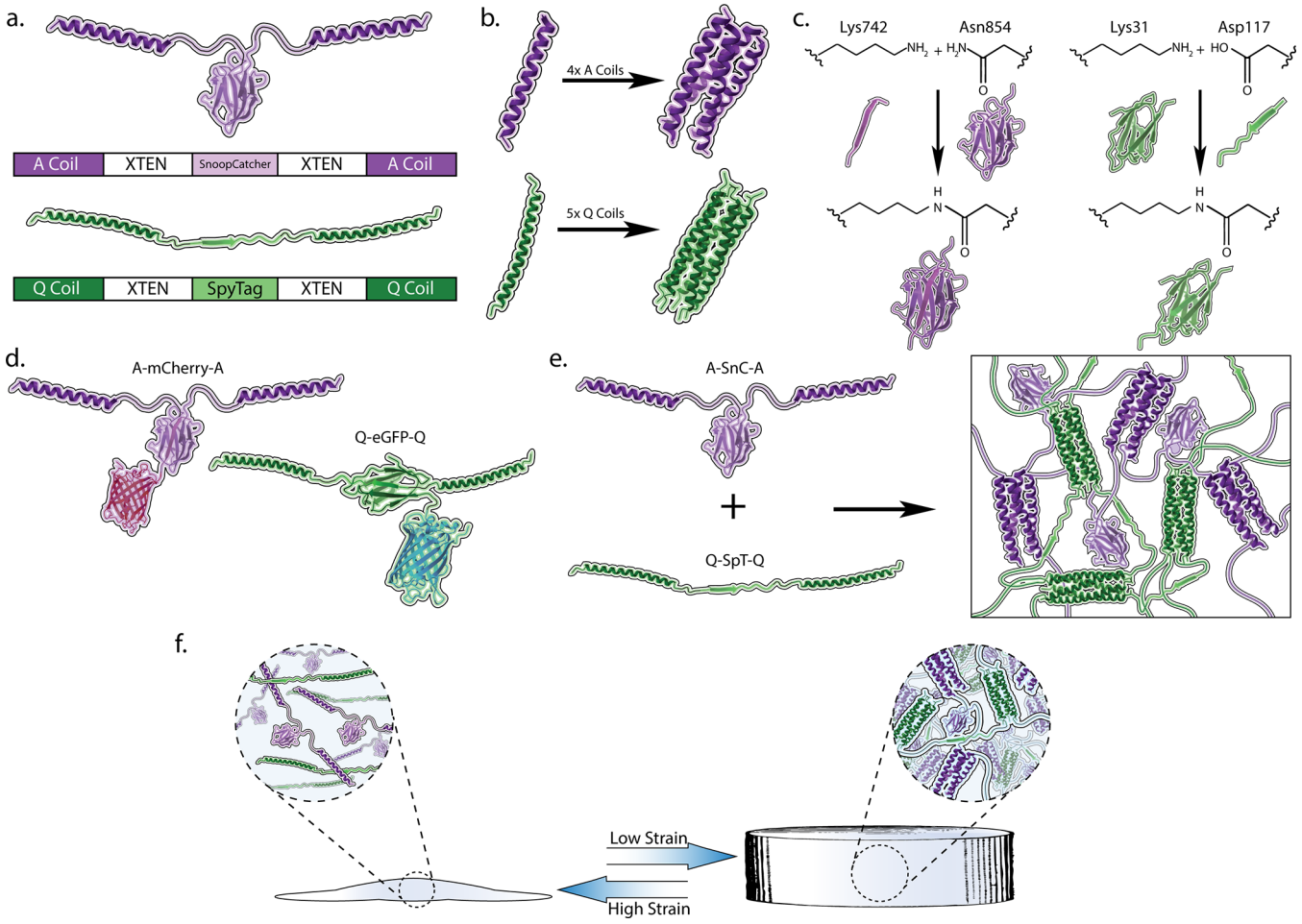

Figure 1. Recombinant protein-based IPN. (a) Diagram and gene block view of A-SnC-A (purple) and Q-SpT-Q (green) telechelic biopolymers. Coil domains flank XTEN bisected by a peptide−protein complexation system to allow for covalent ligation of therapeutics to biopolymers. (b) A coils self-assemble into homotetrameric bundles (top), while Q coils orthogonally form homopentameric coiled-coils (bottom). (c) SnoopLigation yields an isopeptide bond between a critical Lys742 on the SnoopTag and Asn854 on the SnoopCatcher (left), while SpyLigation processed between SpyCatcher's Lys31 and SpyTag's Asp117 (right). (d) The genetically encoded Snoop- and SpyLigation click-like chemistries allow for the covalent tethering of bioactive proteins to the individual network components. Example shows the ligation of mock drugs mCherry-SnT to A-SnC-A (yielding A-mCherry-A, top) and eGFP-SpC to Q-SpT-Q (yielding Q-eGFP-Q, bottom). (e) Upon mixing A-SnC-A and Q-SpT-Q at millimolar concentrations, biopolymers self-sort to form entangled IPN networks. (f) Coiled-coil-forming domains enable the creation of a physically associated hydrogel with shear-thinning and self-healing properties.

batch variability, creating an easier path for FDA approval, and (6) biocompatibility and bioresorbability, such that they can be dissolved within the body into nontoxic byproducts without triggering an immune response or local inflammation.[6,23,25] Unfortunately, most biomaterial strategies to date fail to simultaneously meet all of these requirements.

Interpenetrating polymer networks (IPNs)—materials that contain two or more nonassociating entangled networks—represent an attractive potential solution toward incorporating several desirable traits into a single biomaterial for drug delivery.[26,27] IPNs enable material constructs to be formulated with physicochemical properties contributed from each of their underlying individual networks.[23,26,27] Most previously reported IPNs for therapeutic delivery have been comprised solely of synthetic polymers, with only a few incorporating naturally sourced[28,29] or a secondary recombinant protein-based biopolymer network.[13,30] Synthetic polymer-based networks [e.g., poly(ethylene glycol) (PEG), poly(vinyl alcohol) (PVA)] afford desirable mechanical properties, physicochemical tunability, and ease of functionalization, but have little intrinsic bioactivity, poor biodegradability, high polydispersity, and potential immunogenicity.[6,11,31] On the other hand, naturally sourced biopolymers (e.g., fibrin, elastin) are intrinsically bioactive, biodegradable, and biocompatible, but generally yield materials with poorly tunable mechanics and biofunctionalization alongside often unreconcilable batch-to-batch variability.[6,11,26,31,32] Recombinant protein-based biopolymers unite many of the beneficial properties from both synthetic and natural polymer types, enabling perfect sequence specificity, physicochemical tunability, ease of functionality, as well as high bioactivity, biodegradability, and biocompatibility.[4,5,16] Single-component networks based on recombinant proteins have become of great interest to the materials community including for therapeutic delivery.[5,16,20,25,33,34] To further push the bounds of genetically encoded materials, we sought to design an IPN that formed completely from genetically encoded biopolymers. We hypothesized that this unexplored class of materials could offer exciting opportunities toward creating advanced and highly tunable drug delivery platforms.

https://doi.org/10.1021/acsbiomaterials.5c00813
ACS Biomater. Sci. Eng. 2025, 11, 4869−4880

In this work, we introduce the first reported recombinant protein-based IPN—one whose self-healing, injectable, bioresorbable, and fully defined chemical nature affords unique advantages for therapeutic protein delivery. As designed, the homogeneous biomaterial is composed of two physically cross-linked networks made from orthogonal self-assembling coiled-coil domains (A- or Q-type) connected by the hydrophilic unstructured protein linker XTEN and bisected with either SpyTag003 (SpT) or SnoopCatcher (SnC) for cargo tethering (Figure 1a). Recently utilized by our group to create injectable single-network protein-based biomaterials,[16,35] XTEN is a highly expressed, nonimmunogenic, and chemically stable intrinsically disordered polypeptide evolved previously to "eXTENd" the in vivo half-life of fused peptides/protein therapeutics.[36] Due to sequence specificity and varying number of coils per coiled bundle, the cross-links assemble orthogonally to one another, allowing for the creation of a "self-sorting" IPN (Figure 1b).[37,38] These physically associated cross-links allow for rapid shear-thinning and self-healing behaviors, important for biomaterial injectability.[16,24,37−39] In this new and fully recombinant IPN design, SpT and SnC enable modular and orthogonal network customization with protein therapeutics via SpyLigation/SnoopLigation peptide−protein covalent complexation (Figure 1c,d).[40,41] This approach permits multiple drugs, including fragile growth factors, to be site-specifically and covalently conjugated to networks composed of A-SnC-A or Q-SpT-Q telechelic biopolymers, eliminating the burst release profile commonly associated with hydrogel-entrapped soluble species while maintaining high bioactivity. A-SnC-A and Q-SpT-Q are miscible across all ratios to yield homogeneous IPNs, whereby overall mechanical modulation, erosion, injectability, and biofunctionality stem from the combination of the two underlying protein networks (Figure 1e,f). As biomaterial mechanics can be tuned independently of their erosion and controlled release profiles, we anticipate that these IPNs will serve as valuable tools for drug delivery and broad tissue engineering applications.

EXPERIMENTAL SECTION

Plasmid Construction. Expression plasmids for biopolymers (A-SnC-A and Q-SpT-Q) and fluorescent proteins (mCherry-SnT and eGFP-SpC) were genetically cloned using gBlocks and PCR products for Gibson Assembly. All cloned plasmids were confirmed by Sanger Sequencing (Genewiz, Inc.). Biopolymers contained RGD, a cell-adhesive peptide sequence derived from fibronectin. Plasmids for recombinant human insulin-like growth factor-1 (rhIGF-1)-SpC and recombinant human epidermal growth factor (rhEGF)-SnT were ordered through GenScript. All proteins contained a hexahistidine tag for immobilized metal affinity chromatography (IMAC) purification. Final protein amino acid sequences for all constructs are provided in Supplementary Table S1.

Protein Expression, Purification, and Validation. All plasmids for protein expression were transformed into *Escherichia coli* (*E. coli*, New England Biolabs). Proteins were expressed using standard protein expression protocols. Pelleted cultures were collected and stored at −80 °C until purification.

Cell pellets from large-scale expressions (>3 L) of A-SnC-A and Q-SpT-Q were independently resuspended in lysis buffer and then lysed by microfluidization, a high-throughput cell lysis process. Biopolymers were purified from clarified supernatant via IMAC on nickel Sepharose FF resin on an ÄKTA Avant (Cytiva). Proteins were purified using standard techniques and buffers at room temperature.[42] Elution fractions from multiple rounds of IMAC were pooled and dialyzed in deionized (DI) water at 4 °C.

Cell pellets expressing eGFP-SpC, mCherry-SnT, rhEGF-SnT, and rhIGF-1-SpC were resuspended in lysis buffer and then lysed via sonication. Sonication was the chosen route for small expressions (<3 L). rhIGF-1-SpC underwent denaturing purification, further supplementing all buffers with 6 M urea. Clarified lysate was purified through Nickel-NTA-based IMAC on an ÄKTA Pure (Cytiva). All proteins were purified using standard techniques and buffers at room temperature.[42] Fluorescent proteins were dialyzed in tris-buffered saline at 4 °C. rhIGF-1-SpC was dialyzed in decreasing concentrations of urea, and then both rhIGF-1-SpC and rhEGF-SnT were individually dialyzed against 20 mM Tris and 50 mM NaCl buffer. Biopolymers and fluorescent proteins were lyophilized so they could be easily weighed out during the hydrogel preparation process, while growth factors were supplemented with 10% glycerol and stored at −80 °C until use.

Protein purity was assessed via sodium dodecyl-sulfate polyacrylamide gel electrophoresis (SDS-PAGE), stained with InVision His-Tag In-Gel stain (Thermo Fisher, LC6030), followed by Coomassie Blue (Supplementary Figures S1−S8). Protein molecular mass was determined via liquid chromatography−mass spectrometry (LC-MS, TripleTOF 5600, AB SCIEX) (Supplementary Figures S1−S8).

Native-PAGE. A-SnC-A and Q-SpT-Q were mixed in equal molar concentrations and then incubated overnight at 4 °C. Nondenaturing polyacrylamide gel electrophoresis (Native-PAGE) was performed to preserve any coiled-coil interactions to verify cross-link and peptide−protein covalent complexation orthogonality. The gel was stained with InVision His-Tag In-Gel stain followed by standard Coomassie Blue staining protocol to visualize protein bands.

Biopolymer Ligation Reactions. A-SnC-A and Q-SpT-Q were respectively mixed with mCherry-SnT and eGFP-SpC at a 1:10 molar ratio (fluorescent proteins in excess) and then reacted for 14−16 h at room temperature, until employing size-exclusion chromatography (SEC, HiLoad 26/600 Superdex 75pg) to separate excess fluorescent proteins from the ligated products. Ligated fluorescent biopolymers (denoted as A-mCherry-A and Q-eGFP-Q) were purely isolated. Growth factors rhEGF-SnT and rhIGF-1-SpC were ligated to the biopolymers in a similar process but with a 1:5 molar excess (yielding species denoted A-rhEGF-A and Q-IGF-1-Q). After overnight reaction, the species were dialyzed in deionized water and then maintained at −80 °C until use.

Hydrogel Preparation. Regardless of composition, all gels were formed at constant total molar protein concentration (1.7 mM), identified initially as that which corresponds to a 7.5% weight per volume (w/v) gel of A-SnC-A. Previously lyophilized A-SnC-A and Q-SpT-Q biopolymers were weighed out to determine exact mass, dissolved in 10% ammonium hydroxide, and then mixed in proper ratios to create the appropriate IPN. Fluorescent hydrogels were formed by substituting a portion (0.17 mM) of the A-SnC-A with A-mCherry-A, or Q-SpT-Q with Q-eGFP-Q. Each hydrogel type was lyophilized overnight. Appropriate volumes of 10× PBS were added the next day to form hydrogels and then incubated overnight at 37 °C until use.

Confocal Microscopy. Hydrogels were mounted on a glass slide surrounded by PBS. A Leica Stellaris 5 confocal microscope was used to fluorescently image the biomaterials. The eGFP-modified Q-SpT-Q networks were visualized at an excitation/emission range of 489 nm/494−592 nm and the mCherry-decorated A-SnC-A biomaterials were measured at an excitation/emission range of 587 nm/592−750 nm. Images were processed using Fiji.[43]

Rheological Characterization of Hydrogel Viscoelasticity. Mechanical properties were determined by using an Anton Paar Physica MCR 301 Rheometer with a parallel-plate geometry (8 mm plate diameter, 500 μm gap) with a temperature-controlled water bath (37 °C). Time sweeps (5% shear strain, 30 rad s^{-1}), angular frequency sweeps (5% shear strain, 0.1 to 50 rad s^{-1}), and strain sweeps (1% to 500% shear strain, 30 rad s^{-1}) were performed for all material types in triplicate. All material types then underwent a cyclic self-healing test in triplicate. The test cycles five times between a low shear strain of 5% and a high shear strain of 500% with a constant angular frequency of 30 rad s^{-1}.

https://doi.org/10.1021/acsbiomaterials.5c00813
ACS Biomater. Sci. Eng. 2025, 11, 4869−4880

The average stiffness and shear strain crossover point were calculated from the rheometry data using Microsoft Excel. Each replicate's stiffness value was taken as the average across all time points during the time sweep. Shear strain crossover point was calculated by graphing the linear G' and G'' region, performing a simple linear regression, and then calculating the intersection point. Shear strain sweep, angular frequency sweep, and cyclic self-healing line plots represent average time points between each replicate.

Gel Erosion. Hydrogels (35 μL) were prepared in triplicate as described previously, supplemented with phenylmethylsulfonyl fluoride (PMSF, 0.75 mM) to ensure that material erosion did not proceed via unwanted proteolytic degradation. On day 0, the tubes were filled with 1× PBS containing PMSF. After 1 h, 200 μL of supernatant was removed for day 0 and frozen until analysis. The removed volume was replaced with fresh 1× PBS with PMSF, and the tubes were digitally photographed using an iPhone camera. The sampling process was repeated on days 2, 3, 4, 6, 9, and 11. Supernatant fluorescence was used to determine the hydrogel degradation over time. Standard curves of known A-mCherry-A and Q-eGFP-Q concentrations were utilized to quantify the overall protein concentration in each sample. Fluorescence was detected from samples on a BioTek Synergy H1M plate reader (Agilent) using 485 nm excitation/528 nm emission for eGFP and 590 nm excitation/645 nm emission for mCherry. The cumulative protein released per day was calculated (including the mass of protein removed each day from sampling) to obtain the final values for the percent released over time. Half-life was determined by a custom R script that performs a second-order polynomial fit and then solves for 50% release. This script, as well as graphs of polynomial fits and equations, is provided in the Supporting Information.

Growth Factor Bioactivity Studies. NIH3T3 fibroblasts (ATCC CRL-1658) were cultured in Dulbecco's modified Eagle medium (DMEM) supplemented with 1% penicillin−streptomycin and 10% fetal bovine serum (FBS). Prior to the experiments, cells were serum-starved overnight. Growth factors (rhEGF-SnT or rhIGF-1-SpC), ligated growth factors (A-rhEGF-A or Q-rhIGF-1-Q, prepared as described above), biopolymers (A-SnC-A or Q-SpT-Q), or no additives (control condition) were added to the cells at 100 ng mL^{-1} for 10 min. At this point, M-PER (ThermoFisher, 78501) with a 1× protease inhibitor cocktail (Fisher, PI87785) was added to the cells prior to manual isolation to prevent cytosolic protein degradation. Harvested cells were lysed by using an ultrasonic bath and vortexing. Cell supernatant was collected and frozen at −80 °C. A Pierce Bicinchoninic acid (BCA) Protein Assay (ThermoFisher) was performed, and cell lysate concentration was adjusted to equalize the protein concentration loaded per well. Western blots were performed with standard protocols. Primary antibodies used were antiphospho-p42/44 MAPK, anti-p38 MAPK, or GAPDH. Secondary antibodies tagged with horseradish peroxidase (HRP) were used for chemiluminescent detection of target proteins and imaged on an Azure 600 AZI600 scanner. Blots were stripped and reblocked to stain with a different primary antibody. Band intensities were determined using Fiji, allowing for the calculation of pERK/ERK ratios in Microsoft Excel.[43]

Quantification of Gel-Released Growth Factors via ELISA. Gels (35 μL) were prepared and sampled in the same fashion as the erosion studies, except 100 μg of rhEGF (290 nM) and rhIGF-1 (90 nM) or 25 μg of rhEGF (72.5 nM) and rhIGF-1 (22.5 nM) were added to the appropriate biopolymer solutions, utilizing the methods discussed prior. Growth factors that were ligated to the biopolymers were reacted with the appropriate mass of biopolymers in solution to create 7.5% w/v gels overnight at 4 °C. The biopolymers were dissolved and mixed to make various IPN combinations. The materials were lyophilized and resuspended to create hydrogels (method discussed previously). Samples were collected on days 0, 2, 3, 4, 6, 9, and 11 for enzyme-linked immunosorbent assay (ELISA) analysis. DuoSet ELISA assays for IGF-1 and EGF were performed according to the manufacturer's instructions to determine concentrations of released growth factors over the 11 day period. Plates were read at 450 nm, and data were analyzed in Microsoft Excel and RStudio, similarly to the initial gel erosion studies.

Statistical Analysis. Statistical tests and graphs were completed in GraphPad Prism (version 6). One-way ANOVAs were performed with Tukey's post hoc analysis, $\alpha = 0.05$, $n = 3$, for most analyses. A one-tailed t test was performed to compare the half-life of release between ligated versus unligated drugs for associated material types. A p-value of <0.05 was considered significant. All data presented was performed in experimental triplicate ($n = 3$) with plots displaying the mean ± standard deviation.

■ ETHICAL AND LEGAL COMPLIANCE

All experiments were approved and performed in accordance with the University of Washington's Environmental Health & Safety policies. IRB approval was not required for this study as all experiments were conducted using established cell lines and did not involve human subjects, human-derived materials, or live animals.

■ RESULTS AND DISCUSSION

Section 1: Biopolymer Design, Purification, and Creation. Two genetically encoded orthogonal multiblock *abcba*-type biopolymers were designed and cloned for bacterial expression (denoted A-SnC-A or Q-SpT-Q). Each biopolymer *a* block consisted of a coiled-coil-forming domain (A or Q coils), a 6xHis-tag for IMAC-based purification, and RGD peptide to promote cell adhesion.[16,37,39] The A coils were derived from an artificial leucine zipper and physically associate into homotetrameric coiled-coil bundles, while Q coils were derived from rat cartilage oligomeric matrix protein and self-associate into homopentameric bundles.[16,24,37−39] The A- and Q-type coiled-coil interactions have been previously demonstrated as orthogonal, attributed to sequence specificity and varying number of coils per bundle,[37,38] a feature that we hypothesized could be exploited for IPN creation. At high concentrations, we expected that these coiled-coil interactions would stabilize the material into a physically cross-linked hydrogel that would exhibit both shear-thinning and self-healing behaviors, important properties for injectability.[16,24,37−39] The *b* block was comprised of a 72-residue flexible hydrophilic protein linker called XTEN.[36] XTEN is a nonimmunogenic and intrinsically disordered protein initially evolved to "eXTENd" the circulation half-life of therapeutic proteins and recently exploited by our group for material creation.[16,36] The *c* block consists of peptide−protein click-like chemistry systems (SpyCatcher/Tag003 or SnoopCatcher/Tag) to allow for covalent drug ligation to the biopolymers via isopeptide bond formation.[40,41,44] Importantly, the Spy- and SnoopLigation systems have been demonstrated to be orthogonal, a feature we envisioned exploiting to attach multiple protein drugs to individual networks comprising our IPN.[40] A-SnC-A and Q-SpT-Q biopolymers were recombinantly expressed in *E. coli* and purified using nickel-NTA IMAC on an ÄKTA Pure. All proteins underwent endotoxin removal with Triton X-114 during purification. High yields of pure biopolymers were obtained (>60 mg per L of culture), and expected molecular weights were verified with SDS-PAGE and LC-MS (Supplementary Figures S1−S8).

Toward the creation of the genetically encoded IPN, we first sought to verify that the cross-links and peptide−protein complexations were, in fact, orthogonal. We incubated A-SnC-A and Q-SpT-Q biopolymers in equal molar concentrations overnight and analyzed the samples via nondenaturing Native-PAGE, thereby preserving noncovalent interactions during electrophoretic protein separation. The Native-PAGE showed clear and distinct bands between A-SnC-A and Q-SpT-Q, with

https://doi.org/10.1021/acsbiomaterials.5c00813
ACS Biomater. Sci. Eng. 2025, 11, 4869−4880

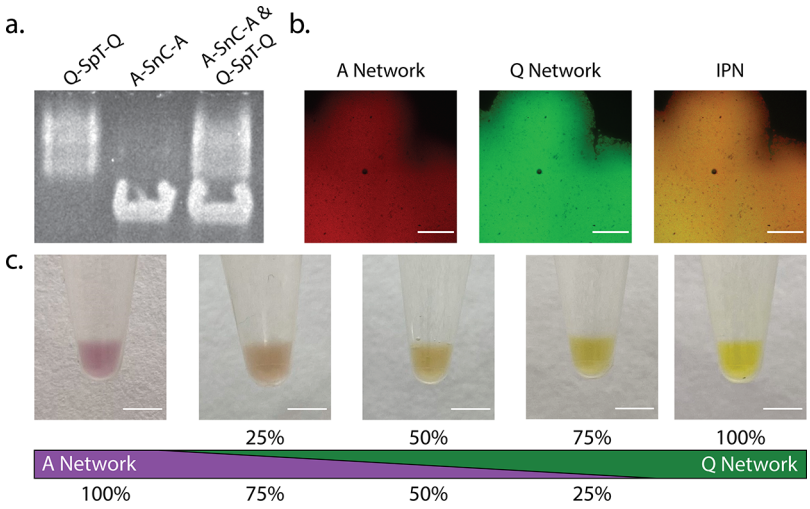

Figure 2. Genetically encoded IPNs form through independent coiled-coil interactions. (a) Native-PAGE of reacted Q-SpT-Q and A-SnC-A indicates orthogonality of the A and Q coil domains and a lack of potential cross-reaction between SpT and SnC. (b) Confocal image of 50% A: 50% Q IPN, whereby 10% of the A network contains A-mCherry-A (0.085 mM) and 10% of the Q network contains Q-eGFP-Q (0.085 mM). Good miscibility and colocalization of both IPN-comprising single networks was observed. Scale bars = 500 μm. (c) Digital photographs of IPNs formed with varying cross-link compositions (0−100% A-SnC-A in Q-SpT-Q, with the A network partially labeled with mCherry and Q with eGFP). Scale bars = 5 mm.

no additional bands observed following extended incubation of the two proteins together (Figure 2a). Consistent with prior reports,[38,40] this study demonstrates that no cross-reactivity occurs between the A- and Q-type coils, as well as that no ligation occurs between SnC and SpT, results we expected would provide a route to create a fully recombinant protein-based IPN.

Encouraged by the observed network component orthogonality, we moved forward with the creation of an IPN. To assess biomaterial homogeneity, we covalently ligated spectrally separated fluorescent proteins mCherry-SnT and enhanced green fluorescent protein (eGFP-SpC) to A-SnC-A and Q-SpT-Q via Snoop- and SpyLigation, respectively, yielding A-mCherry-A and Q-eGFP-Q. When forming a "7.5% w/v" biomaterial, the total molar biopolymer concentration was calculated from a 100% A-SnC-A network (1.7 mM) and held constant across all material types to account for varying biopolymer mass. "A networks" were created with 90% A-SnC-A (1.53 mM) and 10% A-mCherry-A (0.17 mM), while "Q networks" were comprised of 90% Q-SpT-Q (1.53 mM) and 10% Q-eGFP-Q (0.17 mM). When combining A and Q networks to create IPNs, the molar ratios of biopolymers were adjusted to create materials with varying compositions (100%A, 75%A:25%Q, 50%A:50%Q, 25%A:75%Q, and 100%Q) while keeping total protein concentration constant (1.7 mM). For instance, when creating a 75%A:25%Q IPN, 1.275 mM A networks were mixed with 0.425 mM Q networks. To form a hydrogel, polymers were first lyophilized, allowing for the exact mass to be weighed out; these constructs lack aromatic amino acids, inhibiting the accurate protein concentration via UV Absorption spectrophotometry. Polymers were then codissolved in 10% ammonium hydroxide to aid with dissolution and interrupt any preemptive hydrogel formation, ensuring homogeneous mixing. The polymers were subsequently relyophilized at a known mass and reconstituted to create a 7.5% w/v (1.7 mM) IPN hydrogel. Biomaterial homogeneity was inspected by confocal microscopy to determine IPN creation; perfect colocalization of the mCherry and eGFP signals indicated that the IPN was homogeneously formed (Figure 2b). Variation of the IPN composition from 100%A to 100%B (100%A, 75% A:25%Q, 50%A:50%Q, 25%A:75%Q, 100%Q) yielded materials with the expected color gradation, corresponding to different fluorescent cross-link compositions (Figure 2c).

Section 2: Characterization of Biomaterial Viscoelasticity and Injectability. To understand how viscoelastic properties are altered across the variably formulated IPNs, we performed in situ rheological analysis at 37 °C. The stiffness of 7.5% w/v IPNs and individual network hydrogels was measured using a rheological time sweep (5% strain, 30 rad s^{-1}) (Figure 3a). The individual A-SnC-A networks were significantly stiffer (1340 Pa ± 190 Pa) than biomaterials with <75% A coiled-coil cross-links, while the single Q-SpT-Q biomaterials were the softest (380 Pa ± 96 Pa). We propose that this is due to the number of cross-links available per material at equal molar concentrations, where tetrameric bundle-forming A networks can form more cross-links than pentameric bundle-forming Q networks, resulting in stiffer materials. By modulating the cross-link compositions, a near-linear range of intermediate stiffnesses was achieved (Table 1). Substitution of 25% cross-links from a second network lends material stiffness properties to the biomaterial, whereas the stiffness of the 50% A:50% Q IPN neared the mean of the pure individual networks. These demonstrated material stiffness are within the ideal range to mimic native skin, supporting their application for subcutaneous therapeutic depots,[45] and comparable to previously reported coiled-coil cross-linked materials;[16,38,39] in contrast, other recombinant protein-based hydrogels were 2 to 10 times softer than our reported system.[18−20,34,46] By altering the IPN composition, biomaterial stiffness is readily modulated to suit a desired application.

To test biomaterial shear-thinning and self-healing properties, we first performed a strain sweep (10−500% strain, 30 rad s^{-1}) to measure the percent strain at which the biomaterials transition from a primarily elastic ($G' > G''$) to a viscous state ($G'' > G'$) (Supplementary Figure S9). The individual Q-SpT-Q networks had the highest percent strain crossover of 200% ± 13%, indicating that it is the most resistant to strain-induced liquification (Figure 3b, Table 1). In contrast, 100% A-SnC-A

https://doi.org/10.1021/acsbiomaterials.5c00813
ACS Biomater. Sci. Eng. 2025, 11, 4869−4880

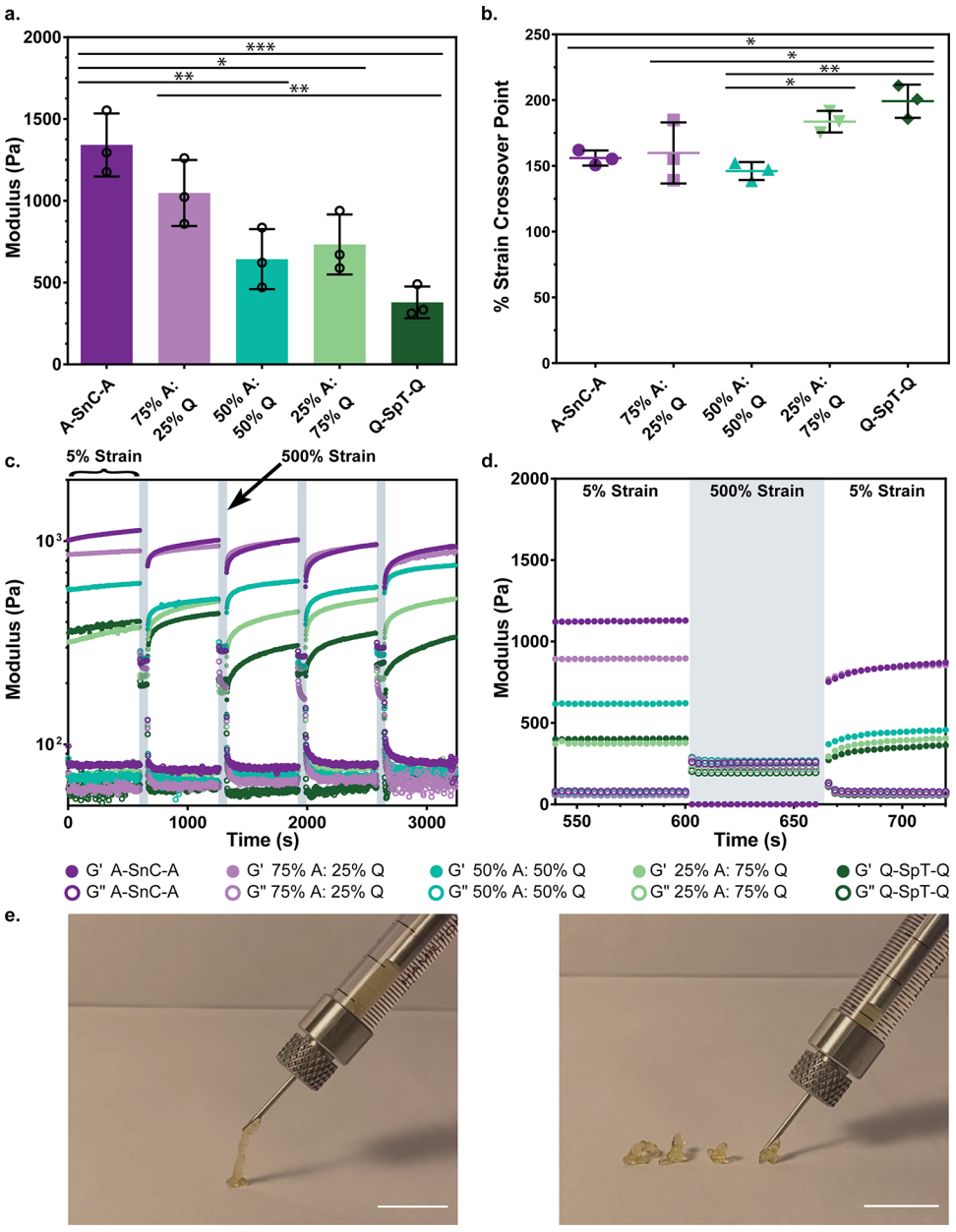

Figure 3. Viscoelastic characterization of IPNs and single-network biomaterials via rheology and syringe injection. (a) Storage modulus (G') for each biomaterial type (5% strain, 30 rad s^{-1}). (b) Percent strain crossover point [loss modulus (G'') > G'] for each biomaterial type (1−500% strain, 30 rad s^{-1}). (c) Cyclic strain test demonstrating shear-thinning and self-healing ability over five cycles of low strain (5%, 30 rad s^{-1}) to high strain (500%, 30 rad s^{-1}, gray shaded boxes). Resolidification of each biomaterial following high-strain removal is rapidly achieved. (d) Zoomed-in view of the first strain cycle (5% strain to 500% strain, gray shaded box, to 5% strain) shown in (c). (e) Injection of 50% A: 50% Q IPN through a 20G needle in a 250 μL Hamilton syringe. Scale bars= 10 mm. All measurements were performed using 7.5% w/v hydrogels at 37 °C. $N = 3$ replicates, bars represent mean ± SD. One-way ANOVA test with Tukey's post hoc analysis, $\alpha = 0.05$. * = $p < 0.05$, ** = $p < 0.005$, *** = $p < 0.0005$. Unless noted on graphs, all other relationships are nonsignificant.

Table 1. Summary of the Rheological Characterization[a]

Biomaterial Composition	A Network	75%A:25%Q	50%A:50%Q	25%A:75%Q	Q Network
Storage Modulus [Pa]	1340 ± 190	1050 ± 200	640 ± 180	730 ± 180	380 ± 100
Strain Crossover [%]	156 ± 6	160 ± 20	146 ± 7	184 ± 8	200 ± 13

[a]Average storage modulus (G') for each biomaterial type (5% strain, 30 rad s^{-1}). Average percent strain crossover point ($G'' > G'$) for each biomaterial type (1−500% strain, 30 rad s^{-1}). All measurements at 37 °C, $n = 3$ replicates, mean ± SD.

biomaterials had a lower percent strain crossover of 156% ± 6%, inversely related to material stiffness trends. The percent strain crossover point for Q-SpT-Q was statistically significant from the percent strain crossover points of the 100% A-SnC-A networks and all IPNs with <75% Q-SpT-Q networks. Interestingly, the 50%A:50%Q IPN had the lowest percent strain crossover point of 146% ± 7%, indicating that the equal combination of cross-link types decreased the biomaterial

https://doi.org/10.1021/acsbiomaterials.5c00813
ACS Biomater. Sci. Eng. 2025, 11, 4869−4880

ductility, while IPNs with at least 75% of a parent cross-link exhibited similar ductility to the parent material. We propose that this trend is observed due to the cross-link characteristics, where more strain is necessary to disassociate pentameric bundles in the Q network versus tetrameric A network bundles. Interestingly, when materials contain equal molar concentration of coiled-coils (e.g., 50%A:50%Q), we predict that a small fraction of coiled-coil bundles are less likely to form proper tetrameric or pentameric bundles, reducing material ductility. Moreover, the supplementation of an alternative network (e.g., 25% cross-links) further decreases the odds of forming bundles from the alternative network, resulting in ductility similar to the parent. Therefore, IPN biomaterial ductility can be modulated by cross-link composition. Additionally, an angular frequency sweep (5% strain, 0.1−50 rad s^{-1}) was performed to determine how cross-link composition impacts the linear viscoelastic range (LVER) of the biomaterials. We observed no crossover for all biomaterial types between an elastic material ($G' > G''$) state to a viscous material ($G'' > G'$) state, indicating that the biomaterials have a large LVER, as seen in previous work for both A and Q coiled-coil cross-linked biomaterials (Supplementary Figure S10).[16,37,38]

Lastly, to assess the biomaterial's self-healing ability over multiple cycles, we performed a cyclic strain test (5 cycles of 5% strain for 200 time points, 3 s each to 500% strain for 20 time points, 3 s each, 30 rad s^{-1}). The strain parameters determined from the aforementioned strain sweep ensured that the biomaterial would be solid at 5% strain but liquefy well before 500% strain for all formulations. Materials were tested for five cycles to demonstrate material durability, where relaxation in between high-strain cycles was 10 min, the minimum time we estimated would take for the material to be loaded into a syringe and subsequently injected in a clinical setting. All material formulations were able to rapidly self-heal upon strain reduction into solid hydrogels, regaining stiffnesses similar to those before liquification by the end of the relaxation periods, indicating maintained network integrity (Figure 3c). Additionally, the stiffness trends across each cycle matched those from the time sweep, as expected. When analyzing the zoomed-in snapshot of the first cycle, it is readily observed that the biomaterials are stable and solid at low strain ($G' > G''$), but under high strain, the biomaterials rapidly liquefy ($G'' > G'$, gray box) (Figure 3d). Upon strain release, the biomaterials were able to near-instantaneously resolidify ($G' > G''$). Past literature is in agreement that high strain disrupts the physical associations between the coiled-coils, liquefying the biomaterial (shear-thinning), while decreased strain allows the coiled-coils to reassemble (self-healing).[16,24] To verify our rheological analysis in a more practical setting, we next tested the shear responsiveness of our genetically encoded IPN through direct injection. A 50%A:50%Q IPN was loaded into a 250 μL Hamilton syringe and injected through a 20G needle (Figure 3e). The IPN liquefied during injection but rapidly resolidified upon exit from the needle, verifying our rheological characterization and visual inspection (Supplementary Video S1). As expected, the creation of an IPN did not disrupt the biomaterials' self-healing and injectable nature.

Section 3: Biomaterial Erosion Properties for Controlled Release. We next sought to determine how cross-link composition impacted the erosion profiles of our biomaterials, which would define the release profile of any tethered therapeutic. As with all physically stabilized networks, coiled-coil-cross-linked materials are subject to surface erosion; as individual coil domains reversibly dissociate from coiled-coil bundles near the surface of the material, they can be diffusively removed from the network and diluted beyond the critical gel-forming concentration.[37,38] As the gel components are released, any ligated therapeutics are also dispersed in the environment at a rate specified by material erosion. Released degradation products include the protein biopolymers (e.g., coiled-coil cross-links, XTEN, and Tag/Catcher systems) and associated covalently ligated drugs. Previous reports have highlighted the biocompatibility and nonimmunogenicity of the various components that comprise our protein biopolymers.[16−18,36] Serving as mock therapeutics whose biomaterial release could be easily quantified by fluorescence, we assessed the erosion of IPNs formed with different ratios of the mCherry-modified A network (i.e., 90% A-SnC-A and 10% A-mCherry-A) and the eGFP-modified Q network (i.e., 90% Q-SpT-Q and 10% Q-eGFP-Q). Lyophilized biopolymers were resuspended to make 7.5% w/v hydrogels in screw cap Eppendorf tubes and incubated in PBS at 37 °C for 11 days (Figure 4a). Gel erosion was assessed

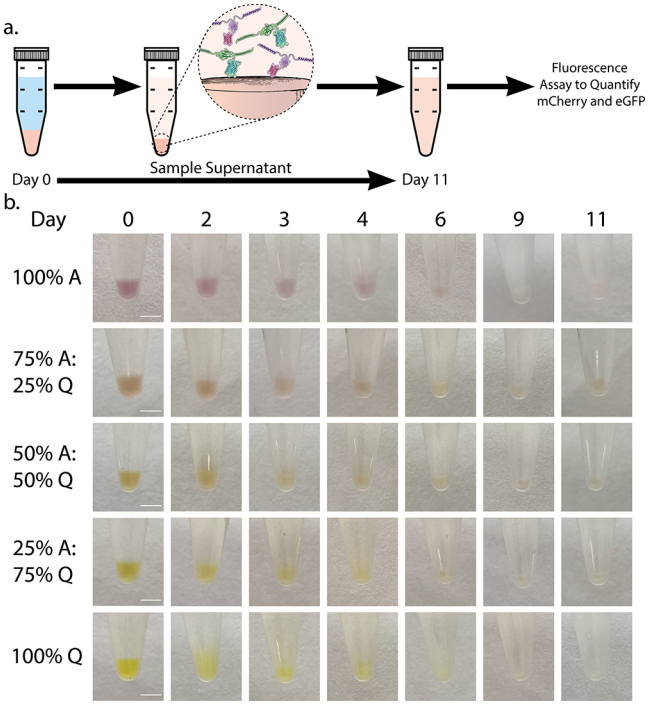

Figure 4. Physical erosion of the IPN and single-network biomaterials over time. (a) Experimental design for determining the biomaterial erosion rate. Hydrogels were cast within tubes. PBS supernatant was sampled over 11 days as the materials underwent surface erosion and then fluorescence of released proteins was quantified. (b) Photographs of each biomaterial type on days 0, 2, 3, 4, 6, 9, and 11 in PBS at 37 °C. Similar erosion profiles were observed across all biomaterials. Here, the A network consists of 90% A-SnC-A and 10% A-mCherry-A and the Q network contains 90% Q-SpT-Q and 10% Q-eGFP-Q; IPNs correspond to a linear combination of each. Scale bars = 5 mm.

using digital photography, while the supernatant was collected to quantify biomaterial erosion and mock drug elution by fluorescence. Initial visual inspection demonstrated that all biomaterial types eroded similarly in the first 6 days, with most biomaterials fully eroded by day 11 (Figure 4b). Notably, these similar rates of erosion were observed across materials with very different viscoelasticities, an important attribute of their potential in vivo deployment.

https://doi.org/10.1021/acsbiomaterials.5c00813
ACS Biomater. Sci. Eng. 2025, 11, 4869−4880

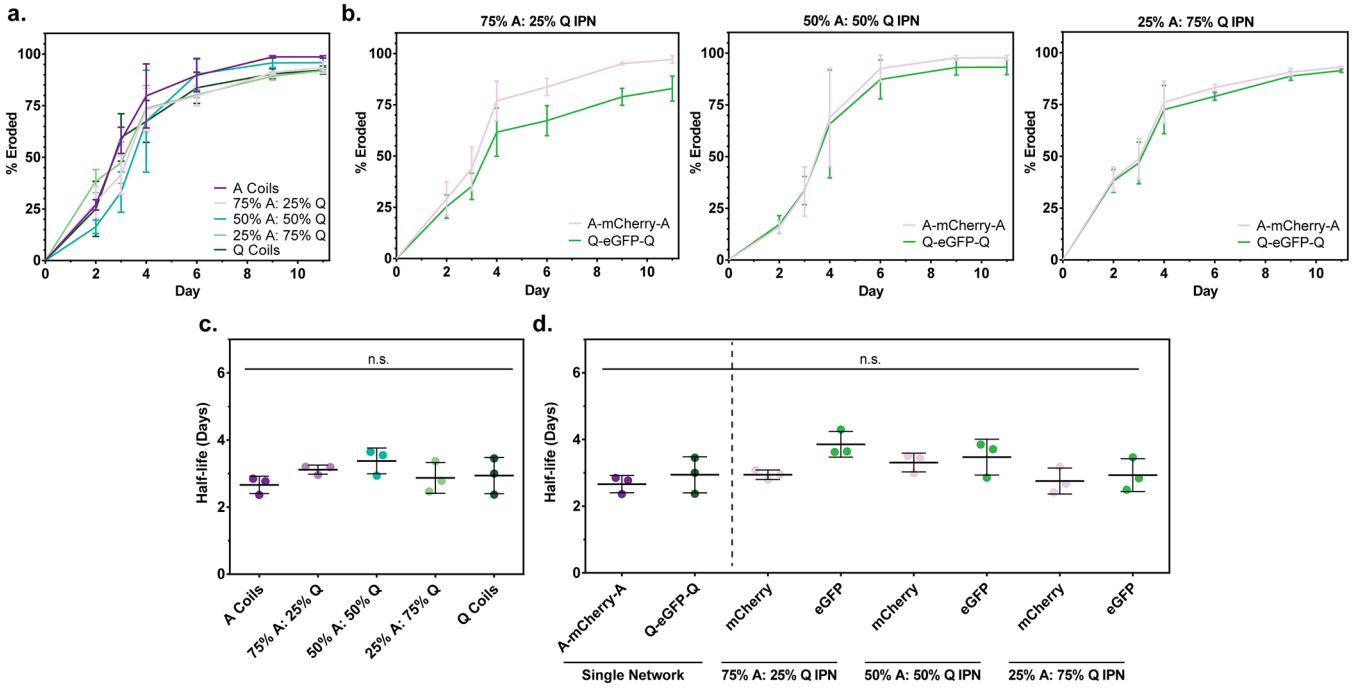

Figure 5. Erosion profiles of single-component and IPN biomaterials. Measurements take advantage of spectrally distinct fluorescent proteins fused to each network (i.e., A-mCherry-A and Q-eGFP-Q). (a) Erosion profiles of total biomaterial erosion for each IPN type compared to single-network materials. (b) IPN-comprising individual networks exhibit similar erosion profiles across a variety of IPN formulations. (c) Half-lives of total biomaterial erosion are similar between single-component networks and various IPNs. (d) Half-lives of each of the IPN-comprising individual networks match those of single-component networks. One-way ANOVA test with Tukey's post hoc analysis, no significance. $N = 3$ replicates, mean ± SD.

Utilizing the spectrally separated and individual network-bound fluorescent cargo (i.e., mCherry and eGFP), we sought to quantify the rate of total material erosion and erosion of each network within the IPNs compared to that of their single-component network counterparts. After gel formulation, the fluorescence of the supernatant (both mCherry and eGFP) was analyzed throughout the 11 day experiment. From these studies, we found that the single-component networks and the various IPNs exhibited no significant difference in rates of total erosion, indicating that cross-linker composition does not significantly impact drug release rates (Figure 5a). The gradual release of almost all the fluorescent protein cargo in 9 days demonstrates the biomaterials' ability to release drugs in a controlled manner, avoiding burst release and achieving erosion-controlled delivery. Taking advantage of the spectrally distinct fluorescent proteins fused to each of the entangled biopolymer networks, we quantified erosion rates and degradation half-lives for each IPN-comprising network across a variety of formulations (Figure 5b–d, Supplementary Table S2–S4, Supplementary Figure S11 and S12). Here, we observed that erosion rates of the IPN-comprising individual networks match both one another as well as that of the single-component systems. We propose that network topology, particularly polymer entanglement, dictates erosion behavior as each polymer must be surface-bound before being able to diffuse into the supernatant, regardless of cross-link composition or mechanical properties, which are primarily driven by cross-link characteristics.

Section 4: Controlled Release of Bioactive Growth Factors. There is growing interest in delivering growth factor therapeutics, such as recombinant human insulin-like growth factor-1 (rhIGF-1) and recombinant human epidermal growth factor (rhEGF), for a variety of applications. As rhEGF can aid with angiogenesis, cellular proliferation, and extracellular matrix remodeling, and rhIGF-1 can stimulate proliferation of fibroblasts, migration of keratinocytes, and expression of collagen,[3] both have utility in the treatment of chronic wounds. When combined, rhEGF and rhIGF-1 have additive effects on wound epithelialization and keratinocyte recruitment, yielding decreased healing times.[3,47,48] Motivated by functional applications in wound healing and to test whether bioactive proteins would retain their activity throughout gel tethering and release, we focused our attention on rhEGF and rhIGF-1 codelivery. We recombinantly expressed rhEGF and rhIGF-1, each with an Fh8 peptide tag to enhance solubility and expression in *E. coli*[49] and a 6xHis-tag for IMAC-assisted purification. rhEGF was expressed with a SnoopTag (referred to as rhEGF-SnT), while rhIGF-1 was fused with a SpyCatcher003 motif (referred to as rhIGF-1-SpC) to allow for covalent ligation to A-SnC-A and Q-SpT-Q, respectively. Upon reaction with the biopolymers, efficient conjugation to the coiled-coil species was observed (Supplementary Figures S13 and S14). To assess whether growth factor bioactivity was retained following ligation to the network-forming biopolymers, we examined each species' ability to drive phosphorylation of extracellular-regulated kinase (pERK) in the mitogen-activated protein kinase (MAPK)/ERK signaling pathway (Figure 6a).[48,50] Upon the addition of ligated and unligated rhEGF-SnT and rhIGF-1-SpC to NIH3T3 fibroblasts, ERK phosphorylation was significantly enhanced compared to that of untreated cells and those treated with unligated biopolymers (A-SnC-A and Q-SpT-Q) (Figure 6b,c). No significant differences were observed between the ligated and unligated growth factors, indicating that bioactivity is not diminished by covalent ligation to the coiled-coil biopolymers, matching previously reported materials that demonstrated that

https://doi.org/10.1021/acsbiomaterials.5c00813
ACS Biomater. Sci. Eng. 2025, 11, 4869–4880

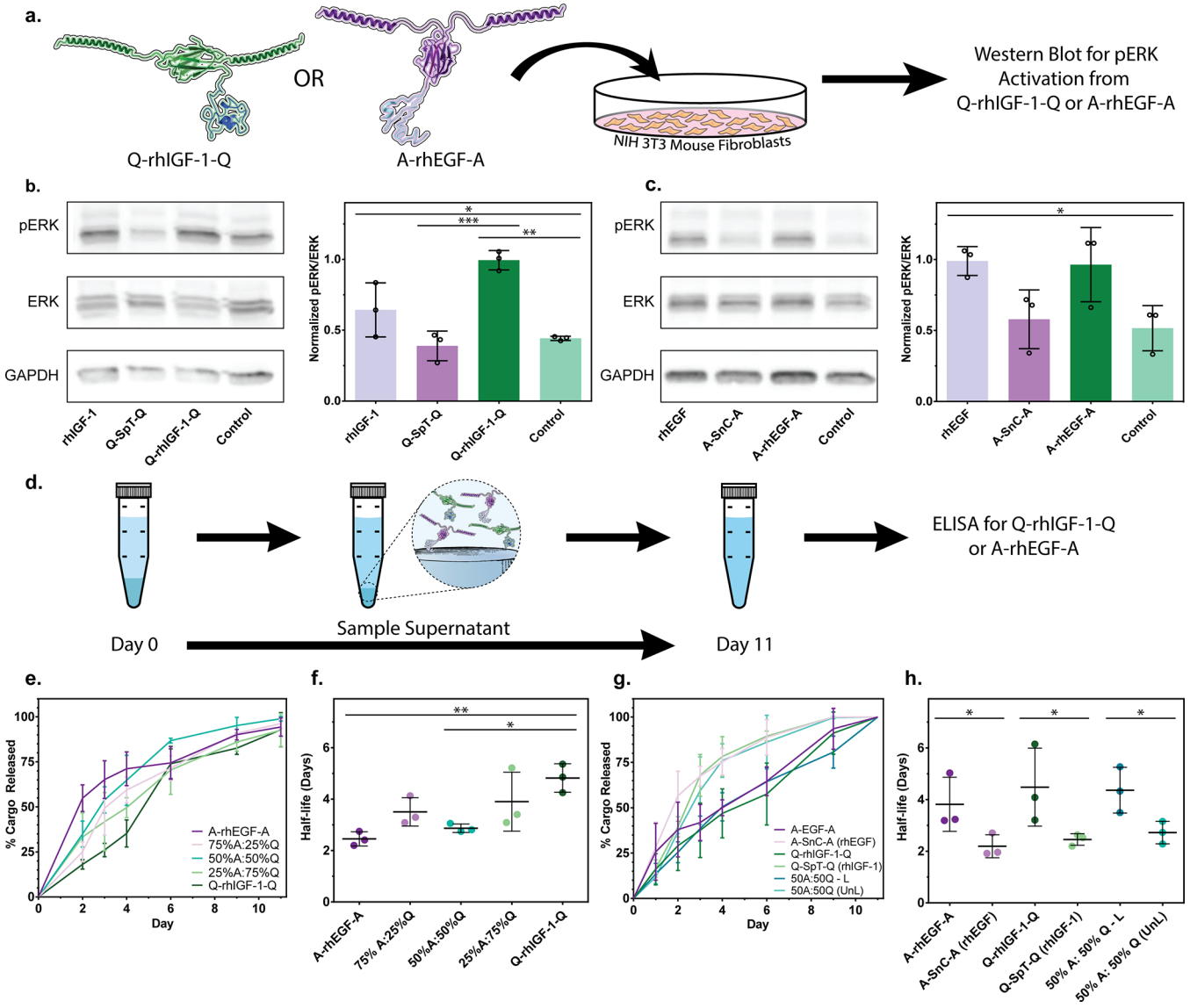

Figure 6. Growth factors maintain high bioactivity following biopolymer tethering and controlled release. (a) Growth factors rhIGF-1 and rhEGF were covalently ligated to biopolymers, and their bioactivity tested by pERK activation in the MAPK/ERK pathway in NIH3T3 fibroblasts. pERK was detected via Western blot. (b) Western blot and bioactivity quantification of untethered rhEGF-SnT, A-SnC-A, A-rhEGF-A, and untreated controls. (c) Western blot and bioactivity quantification of untethered rhIGF-1-SpC, Q-SpT-Q, Q-rhIGF-1-Q and untreated controls. (d) Experimental design for biomaterial release of growth factors. Hydrogels with appropriate tethered growth factors were cast into tubes. The PBS supernatant was sampled until day 11, and then ELISAs for individual growth factor detection were performed. (e) Total growth factor elution profiles for each IPN type compared to single-network materials. (f) Half-life of total drug release is similar between single-component networks and the various IPNs. One-way ANOVA test with Tukey's post hoc analysis. Unless noted on graphs, all other relationships are nonsignificant. (g) Release profiles of growth factors when covalently tethered (dark colors) versus untethered (light colors). (h) Half-life of drug release between tethered and untethered growth factors. One-tailed t test were performed between associated materials with tethered and untethered GFs. All experiments were performed with $N = 3$ replicates, bars represent mean ± SD. Western blot quantification normalized to GAPDH and ratio of control group. α=0.05. *=$p < 0.05$, **=$p < 0.005$, ***=$p < 0.0005$.

ligated therapeutics remained bioactive and even had superior activity compared to genetically fused therapeutics.[13,17]

Heartened by findings that rhEGF and rhIGF-1 growth factors retained high bioactivity following biopolymer conjugation, we next sought to control their release from our engineered biomaterials. A networks were ligated with 100 μg of rhEGF-SnT (17.0% biopolymers conjugated, 290 nM), while Q networks were ligated with 100 μg of rhIGF-SpC (5.2% biopolymers conjugated, 90 nM) and then formed into 35 μL gels as described above, to be incubated over 11 days in PBS at 37 °C (Figure 6d). The supernatant was collected on days 0, 2, 3, 4, 6, 9, and 11, and then ELISA assays specific to rhIGF-1 and rhEGF were utilized to track individual drug elution over time. The IPNs released their cargo in a steady and controlled manner with no burst release over a 10 day period, consistent with initial material erosion studies involving fluorescent cargo (Figure 6e). When analyzing the release profiles for A-rhEGF-A and Q-rhIGF-1-Q networks within one IPN type, we found that both drugs coeluted at matching rates across all material types (Supplementary Figure S15). Additionally, the half-life of growth factor release was relatively similar to the half-life of fluorescent protein release in the initial erosion study, ranging

https://doi.org/10.1021/acsbiomaterials.5c00813
ACS Biomater. Sci. Eng. 2025, 11, 4869−4880

between 2.5 ± 0.3 days to 4.8 ± 0.6 days for A- and Q-networks, respectively (Figure 6f, Supplementary Tables S5 and S6, Supplementary Figure S16). Interestingly, Q-rhIGF-1-Q biomaterials had an extended half-life of 4.8 ± 0.6 days and were statistically significant from the half-life release of A-rhEGF-A, while the IPNs spanned the half-life range between the single-component biomaterials. The half-lives of underlying networks (A-rhEGF-A and Q-rhIGF-1-Q) comprising each IPN were statistically similar to each other for all IPN types, verifying that drug elution per network occurs in a controlled manner regardless of material (Supplementary Tables S5 and S7, Supplementary Figures S15 and S17). Gel-released growth factors remained bioactive throughout the entire 11 day experiment (Supplementary Figure S18). Importantly, such similar rates of therapeutic cargo release were observed across materials with tunable viscoelasticity (shown in Figure 3). Since injected material stiffness plays an important role in its eventual in vivo function, we expect this to be a critical improvement over the use of a single-component protein hydrogel.

To further underscore the uniqueness of our system's ability to deliver protein drugs in a controlled manner via covalent ligation to the biopolymers, we delivered growth factors either covalently ligated to our system or untethered (i.e., growth factors without Tag/Catcher chemistries simply entrapped within the hydrogels) for single-network and 50%A:50%Q IPN materials. Gels (35 μL) were loaded with rhEGF (25 μg, 4.3% biopolymers conjugated −72.5 nM), while Q networks were loaded with rhIGF-1 (25 μg, 1.3% biopolymers conjugated −22.5 nM). The *in vitro* drug delivery study was conducted as described above in cell media (free of protease inhibitors or antibiotics) with time-dependent release quantified via ELISA. In these studies, we found that growth factors ligated to the network components exhibited significantly prolonged release compared to untethered growth factors when analyzing the cumulative release profiles and half-life of total drug release (Figure 6g,h, Supplementary Tables S8 and S9, Supplementary Figure S19). These differences can be further observed when analyzing the release profiles and the half-life of drug release for the independent networks within the 50%A:50%Q IPN (Supplementary Tables S8 and S10, Supplementary Figures S20−S21). This study underscores that covalent ligation of therapeutics prolongs drug delivery compared to strategies reliant on simple diffusion for delivery, consistent with reports elsewhere.[17,19,20] One observation of note is that drug release seemed to be extended for tethered growth factors compared to previous studies, attributed to an inclusion of a lower percentage of tethered drugs with low molecular weights, resulting in less disruption of cross-link formation. Taken together, these results demonstrate that our genetically encoded IPNs were able to release therapeutically relevant and bioactive protein cargos from materials in a controlled manner.

CONCLUSIONS

In this paper, we have introduced a fully genetically encoded IPN biomaterial that exhibits many desirable criteria for therapeutic protein drug delivery. Homogeneously mixed IPNs were successfully created, allowing for the exploration of material properties in response to network composition. Biomaterial viscoelasticity was readily tuned based on cross-link composition while maintaining controlled release of up to two therapeutically relevant cargoes for 10 days. IPNs retained their shear-thinning and self-healing properties as expected, allowing for injectability. Additionally, we demonstrated that the covalent ligation of recombinant therapeutics to the biopolymers did not disrupt material formation or cargo bioactivity, allowing for drug elution dependent on material erosion to prevent a burst release profile often seen with hydrogel reservoirs. Tethered growth factors were slowly released over 10 days in similar release profiles as seen with mock fluorescent drugs, underscoring these materials' abilities to release drugs in a controlled manner, regardless of the cargo. Ongoing efforts in our group have demonstrated that alternative materials cross-linked via coiled-coils can be successfully injected in vivo and remain intact well beyond 3 days, underscoring the stability of physically associated recombinant protein materials in vivo.[16] Additionally, others in our group are utilizing de novo-designed protein multimerization as a secondary gelation chemistry that, when combined with the A or Q coils, will afford an even wider range of material properties and therapeutic release.[51] We anticipate that these biomaterials will be useful for the therapeutic delivery of protein drugs and broad tissue engineering applications.

ASSOCIATED CONTENT

Supporting Information

The Supporting Information is available free of charge at https://pubs.acs.org/doi/10.1021/acsbiomaterials.5c00813.

Detailed methods, amino acid sequences for all protein constructs, and data for additional protein characterization and gel rheological analysis (PDF)

50%A:50%Q IPN loaded into a 250 μL Hamilton syringe and injected through a 20G needle (MOV)

AUTHOR INFORMATION

Corresponding Author

Cole A. DeForest − *Department of Bioengineering, Institute for Protein Design, Department of Chemical Engineering, Department of Chemistry, and Molecular Engineering & Sciences Institute, University of Washington, Seattle, Washington 98105, United States; Institute of Stem Cell & Regenerative Medicine, University of Washington, Seattle, Washington 98109, United States;* orcid.org/0000-0003-0337-3577; Email: profcole@uw.edu

Authors

Murial L. Ross − *Department of Bioengineering, University of Washington, Seattle, Washington 98105, United States;* orcid.org/0000-0001-6878-6714

Shivani P. Kottantharayil − *Department of Bioengineering, University of Washington, Seattle, Washington 98105, United States;* orcid.org/0009-0001-4916-4706

Tina K. Nguyen − *Institute for Protein Design and Department of Biochemistry, University of Washington, Seattle, Washington 98105, United States*

Rashmi Ravichandran − *Institute for Protein Design, University of Washington, Seattle, Washington 98105, United States;* orcid.org/0000-0002-2630-7487

Complete contact information is available at: https://pubs.acs.org/10.1021/acsbiomaterials.5c00813

Funding

This work was further supported by a Maximizing Investigators' Research Award (R35GM138036, C.A.D.) from the National Institutes of Health. Student fellowship support was provided from the National Science Foundation (DGE-2140004,

M.L.R.), Washington NASA Space Grant Consortium (80NSSC20M0104, S.P.K.), and the UW Mary Gates Endowment for Students (S.P.K.).

Notes

The authors declare no competing financial interest.

■ ACKNOWLEDGMENTS

The authors gratefully acknowledge Dale Whittington for training and maintenance of the UW Mass Spectrometry Center. In addition, part of this work was conducted with instrumentation provided by the Joint Center for Deployment and Research in Earth Abundant Materials (JCDREAM).

■ REFERENCES

(1) Jayakrishnan, A.; Wan Rosli, W. R.; Tahir, A. R. M.; Razak, F. S. A.; Kee, P. E.; Ng, H. S.; Chew, Y. L.; Lee, S. K.; Ramasamy, M.; Tan, C. S.; Liew, K. B. Evolving Paradigms of Recombinant Protein Production in Pharmaceutical Industry: A Rigorous Review. *Sci.* **2024**, *6* (1), 9.

(2) Lagassé, H. A. D.; Alexaki, A.; Simhadri, V. L.; Katagiri, N. H.; Jankowski, W.; Sauna, Z. E.; Kimchi-Sarfaty, C. Recent Advances in (Therapeutic Protein) Drug Development. *F1000Research* **2017**, *6*, 113.

(3) Dolati, S.; Yousefi, M.; Pishgahi, A.; Nourbakhsh, S.; Pourabbas, B.; Shakouri, S. K. Prospects for the Application of Growth Factors in Wound Healing. *Growth Factors Chur Switz.* **2020**, *38* (1), 25−34.

(4) Garcia, C. G.; Patkar, S. S.; Wang, B.; Abouomar, R.; Kiick, K. L. Recombinant Protein-Based Injectable Materials for Biomedical Applications. *Adv. Drug Delivery Rev.* **2023**, *193*, No. 114673.

(5) Frandsen, L.; Ghandehari, J. Recombinant Protein-Based Polymers for Advanced Drug Delivery. *Chem. Soc. Rev.* **2012**, *41* (7), 2696−2706.

(6) Subbiah, R.; Guldberg, R. E. Materials Science and Design Principles of Growth Factor Delivery Systems in Tissue Engineering and Regenerative Medicine. *Adv. Healthc. Mater.* **2019**, *8* (1), No. e1801000.

(7) Saghazadeh, S.; Rinoldi, C.; Schot, M.; Kashaf, S. S.; Sharifi, F.; Jalilian, E.; Nuutila, K.; Giatsidis, G.; Mostafalu, P.; Derakhshandeh, H.; Yue, K.; Swieszkowski, W.; Memic, A.; Tamayol, A.; Khademhosseini, A. Drug Delivery Systems and Materials for Wound Healing Applications. *Adv. Drug Delivery Rev.* **2018**, *127*, 138−166.

(8) Wang, J.; Song, Y.; Xie, W.; Zhao, J.; Wang, Y.; Yu, W. Therapeutic Angiogenesis Based on Injectable Hydrogel for Protein Delivery in Ischemic Heart Disease. *iScience* **2023**, *26* (5), No. 106577.

(9) Wang, Z.; Wang, Z.; Lu, W. W.; Zhen, W.; Yang, D.; Peng, S. Novel Biomaterial Strategies for Controlled Growth Factor Delivery for Biomedical Applications. *NPG Asia Mater.* **2017**, *9* (10), e435−e435.

(10) Nealy, E. S.; Reed, S. J.; Adelmund, S. M.; Badeau, B. A.; Shadish, J. A.; Girard, E. J.; Brasel, K.; Pakiam, F. J.; Mhyre, A. J.; Price, J. P.; Sarkar, S.; Kalia, V.; DeForest, C. A.; Olson, J. M. Versatile Tissue-injectable Hydrogels Capable of the Extended Hydrolytic Release of Bioactive Protein Therapeutics. *Bioeng. Transl. Med.* **2024**, *9* (5), No. e10668.

(11) Gharios, R.; Francis, R. M.; DeForest, C. A. Chemical and Biological Engineering Strategies to Make and Modify Next-Generation Hydrogel Biomaterials. *Matter* **2023**, *6* (12), 4195−4244.

(12) Barrett-Catton, E.; Ross, M. L.; Asuri, P. Multifunctional Hydrogel Nanocomposites for Biomedical Applications. *Polymers* **2021**, *13* (6), No. 856.

(13) Wang, J.; Li, J.; Sun, Y.; Liu, X.; Wang, L.; Xia, Y.; Huang, J.; Feng, J.; Jia, S.; Li, Y.; Guo, Z.; Dong, Y.; Wang, L.; Li, X. Genetically Encoded Incorporation of IFN-α into Collagen-like Protein-Hyaluronic Acid Hydrogels for Diabetic Chronic Wound Healing. *ACS Mater. Lett.* **2024**, *6* (9), 4133−4141.

(14) Jia, S.; Wang, J.; Wang, X.; Liu, X.; Li, S.; Li, Y.; Li, J.; Wang, J.; Man, S.; Guo, Z.; Sun, Y.; Jia, Z.; Wang, L.; Li, X. Genetically Encoded in Situ Gelation Redox-Responsive Collagen-like Protein Hydrogel for Accelerating Diabetic Wound Healing. *Biomater. Sci.* **2023**, *11* (24), 7748−7758.

(15) Duraj-Thatte, A. M.; Courchesne, N.-M. D.; Praveschotinunt, P.; Rutledge, J.; Lee, Y.; Karp, J. M.; Joshi, N. S. Genetically Programmable Self-Regenerating Bacterial Hydrogels. *Adv. Mater.* **2019**, *31* (40), No. 1901826.

(16) Bennett, J. I.; Boit, M. O.; Gregorio, N. E.; Zhang, F.; Kibler, R. D.; Hoye, J. W.; Prado, O.; Rapp, P. B.; Murry, C. E.; Stevens, K. R.; DeForest, C. A. Genetically Encoded XTEN-Based Hydrogels with Tunable Viscoelasticity and Biodegradability for Injectable Cell Therapies. *Adv. Sci.* **2024**, *11* (24), No. 2301708.

(17) Li, Y.; Yang, C.; Fang, S.; Zhou, Y.; Li, M.; Liu, Z.; Zhang, X.; Duan, L.; Liu, K.; Sun, F. Clickable, Thermally Responsive Hydrogels Enabled by Recombinant Spider Silk Protein and Spy Chemistry for Sustained Neurotrophin Delivery. *Adv. Mater.* **2025**, *37*, No. 2413957.

(18) Sun, F.; Zhang, W.-B.; Mahdavi, A.; Arnold, F. H.; Tirrell, D. A. Synthesis of Bioactive Protein Hydrogels by Genetically Encoded SpyTag-SpyCatcher Chemistry. *Proc. Natl. Acad. Sci. U. S. A.* **2014**, *111* (31), 11269−11274.

(19) Asai, D.; Xu, D.; Liu, W.; Garcia Quiroz, F.; Callahan, D. J.; Zalutsky, M. R.; Craig, S. L.; Chilkoti, A. Protein Polymer Hydrogels by *in Situ*, Rapid and Reversible Self-Gelation. *Biomaterials* **2012**, *33* (21), 5451−5458.

(20) Hill, L. K.; Meleties, M.; Katyal, P.; Xie, X.; Delgado-Fukushima, E.; Jihad, T.; Liu, C.-F.; O'Neill, S.; Tu, R. S.; Renfrew, P. D.; Bonneau, R.; Wadghiri, Y. Z.; Montclare, J. K. Thermoresponsive Protein-Engineered Coiled-Coil Hydrogel for Sustained Small Molecule Release. *Biomacromolecules* **2019**, *20* (9), 3340−3351.

(21) Gao, X.; Fang, J.; Xue, B.; Fu, L.; Li, H. Engineering Protein Hydrogels Using SpyCatcher-SpyTag Chemistry. *Biomacromolecules* **2016**, *17* (9), 2812−2819.

(22) Sisso, A. M.; Boit, M. O.; DeForest, C. A. Self-Healing Injectable Gelatin Hydrogels for Localized Therapeutic Cell Delivery. *J. Biomed. Mater. Res., Part A* **2020**, *108* (5), 1112−1121.

(23) Bertsch, P.; Diba, M.; Mooney, D. J.; Leeuwenburgh, S. C. G. Self-Healing Injectable Hydrogels for Tissue Regeneration. *Chem. Rev.* **2023**, *123*, 834.

(24) Olsen, B. D.; Kornfield, J. A.; Tirrell, D. A. Yielding Behavior in Injectable Hydrogels from Telechelic Proteins. *Macromolecules* **2010**, *43* (21), 9094−9099.

(25) Varanko, A.; Saha, S.; Chilkoti, A. Recent Trends in Protein and Peptide-Based Biomaterials for Advanced Drug Delivery. *Adv. Drug Delivery Rev.* **2020**, *156*, 133−187.

(26) Dhand, A. P.; Galarraga, J. H.; Burdick, J. A. Enhancing Biopolymer Hydrogel Functionality through Interpenetrating Networks. *Trends Biotechnol.* **2021**, *39* (5), 519−538.

(27) Bidault, L.; Deneufchatel, M.; Hindié, M.; Vancaeyzeele, C.; Fichet, O.; Larreta-Garde, V. Fibrin-Based Interpenetrating Polymer Network Biomaterials with Tunable Biodegradability. *Polymer* **2015**, *62*, 19−27.

(28) Naseri, N.; Deepa, B.; Mathew, A. P.; Oksman, K.; Girandon, L. Nanocellulose-Based Interpenetrating Polymer Network (IPN) Hydrogels for Cartilage Applications. *Biomacromolecules* **2016**, *17* (11), 3714−3723.

(29) Zou, Z.; Zhang, B.; Nie, X.; Cheng, Y.; Hu, Z.; Liao, M.; Li, S. A Sodium Alginate-Based Sustained-Release IPN Hydrogel and Its Applications. *RSC Adv.* **2020**, *10* (65), 39722−39730.

(30) Dai, Z.; Yang, X.; Wu, F.; Wang, L.; Xiang, K.; Li, P.; Lv, Q.; Tang, J.; Dohlman, A.; Dai, L.; Shen, X.; You, L. Living Fabrication of Functional Semi-Interpenetrating Polymeric Materials. *Nat. Commun.* **2021**, *12* (1), 3422.

(31) Reddy, M. S. B.; Ponnamma, D.; Choudhary, R.; Sadasivuni, K. K. A Comparative Review of Natural and Synthetic Biopolymer Composite Scaffolds. *Polymers* **2021**, *13* (7), No. 1105.

(32) Zhang, Y.; Liu, J.; Huang, L.; Wang, Z.; Wang, L. Design and Performance of a Sericin-Alginate Interpenetrating Network Hydrogel for Cell and Drug Delivery. *Sci. Rep.* **2015**, *5* (1), No. 12374.

(33) Lindsey, S.; Piatt, J. H.; Worthington, P.; Sönmez, C.; Satheye, S.; Schneider, J. P.; Pochan, D. J.; Langhans, S. A. Beta Hairpin Peptide

https://doi.org/10.1021/acsbiomaterials.5c00813
ACS Biomater. Sci. Eng. 2025, 11, 4869−4880

Hydrogels as an Injectable Solid Vehicle for Neurotrophic Growth Factor Delivery. *Biomacromolecules* **2015**, *16* (9), 2672−2683.
(34) Wong Po Foo, C. T. S.; Lee, J. S.; Mulyasasmita, W.; Parisi-Amon, A.; Heilshorn, S. C. Two-Component Protein-Engineered Physical Hydrogels for Cell Encapsulation. *Proc. Natl. Acad. Sci. U. S. A.* **2009**, *106* (52), 22067−22072.
(35) Gregorio, N. E.; DeForest, C. A. PhoCoil: An Injectable and Photodegradable Single-Component Recombinant Protein Hydrogel for Localized Therapeutic Cell Delivery. *bioRxiv* **2024**, 2024.05.07.592971.
(36) Schellenberger, V.; Wang, C.; Geething, N. C.; Spink, B. J.; Campbell, A.; To, W.; Scholle, M. D.; Yin, Y.; Yao, Y.; Bogin, O.; Cleland, J. L.; Silverman, J.; Stemmer, W. P. C. A Recombinant Polypeptide Extends the in Vivo Half-Life of Peptides and Proteins in a Tunable Manner. *Nat. Biotechnol.* **2009**, *27* (12), 1186−1190.
(37) Dooling, L. J.; Tirrell, D. A. Engineering the Dynamic Properties of Protein Networks through Sequence Variation. *ACS Cent. Sci.* **2016**, *2* (11), 812−819.
(38) Shen, W.; Zhang, K.; Kornfield, J. A.; Tirrell, D. A. Tuning the Erosion Rate of Artificial Protein Hydrogels through Control of Network Topology. *Nat. Mater.* **2006**, *5* (2), 153−158.
(39) Shen, W.; Kornfield, J. A.; Tirrell, D. A. Structure and Mechanical Properties of Artificial Protein Hydrogels Assembled through Aggregation of Leucine Zipper Peptide Domains. *Soft Matter* **2007**, *3* (1), 99−107.
(40) Veggiani, G.; Nakamura, T.; Brenner, M. D.; Gayet, R. V.; Yan, J.; Robinson, C. V.; Howarth, M. Programmable Polyproteams Built Using Twin Peptide Superglues. *Proc. Natl. Acad. Sci. U. S. A.* **2016**, *113* (5), 1202−1207.
(41) Keeble, A. H.; Turkki, P.; Stokes, S.; Khairil Anuar, I. N. A.; Rahikainen, R.; Hytönen, V. P.; Howarth, M. Approaching Infinite Affinity through Engineering of Peptide-Protein Interaction. *Proc. Natl. Acad. Sci. U. S. A.* **2019**, *116* (52), 26523−26533.
(42) Structural Genomics Consortium; China Structural Genomics Consortium; Northeast Structural Genomics Consortium; Gräslund, S.; Nordlund, P.; Weigelt, J.; Hallberg, B. M.; Bray, J.; Gileadi, O.; Knapp, S.; Oppermann, U.; Arrowsmith, C.; Hui, R.; Ming, J.; dhe-Paganon, S.; Park, H.; Savchenko, A.; Yee, A.; Edwards, A.; Vincentelli, R.; Cambillau, C.; Kim, R.; Kim, S.-H.; Rao, Z.; Shi, Y.; Terwilliger, T. C.; Kim, C.-Y.; Hung, L.-W.; Waldo, G. S.; Peleg, Y.; Albeck, S.; Unger, T.; Dym, O.; Prilusky, J.; Sussman, J. L.; Stevens, R. C.; Lesley, S. A.; Wilson, I. A.; Joachimiak, A.; Collart, F.; Dementieva, I.; Donnelly, M. I.; Eschenfeldt, W. H.; Kim, Y.; Stols, L.; Wu, R.; Zhou, M.; Burley, S. K.; Emtage, J. S.; Sauder, J. M.; Thompson, D.; Bain, K.; Luz, J.; Gheyi, T.; Zhang, F.; Atwell, S.; Almo, S. C.; Bonanno, J. B.; Fiser, A.; Swaminathan, S.; Studier, F. W.; Chance, M. R.; Sali, A.; Acton, T. B.; Xiao, R.; Zhao, L.; Ma, L. C.; Hunt, J. F.; Tong, L.; Cunningham, K.; Inouye, M.; Anderson, S.; Janjua, H.; Shastry, R.; Ho, C. K.; Wang, D.; Wang, H.; Jiang, M.; Montelione, G. T.; Stuart, D. I.; Owens, R. J.; Daenke, S.; Schütz, A.; Heinemann, U.; Yokoyama, S.; Büssow, K.; Gunsalus, K. C. Protein Production and Purification. *Nat. Methods* **2008**, *5* (2), 135−146.
(43) Schindelin, J.; Arganda-Carreras, I.; Frise, E.; Kaynig, V.; Longair, M.; Pietzsch, T.; Preibisch, S.; Rueden, C.; Saalfeld, S.; Schmid, B.; Tinevez, J.-Y.; White, D. J.; Hartenstein, V.; Eliceiri, K.; Tomancak, P.; Cardona, A. Fiji: An Open-Source Platform for Biological-Image Analysis. *Nat. Methods* **2012**, *9* (7), 676−682.
(44) Zakeri, B.; Fierer, J. O.; Celik, E.; Chittock, E. C.; Schwarz-Linek, U.; Moy, V. T.; Howarth, M. Peptide Tag Forming a Rapid Covalent Bond to a Protein, through Engineering a Bacterial Adhesin. *Proc. Natl. Acad. Sci. U. S. A.* **2012**, *109* (12), E690−E697.
(45) Xie, C.; Liu, G.; Wang, L.; Yang, Q.; Liao, F.; Yang, X.; Xiao, B.; Duan, L. Synthesis and Properties of Injectable Hydrogel for Tissue Filling. *Pharmaceutics* **2024**, *16* (3), No. 430.
(46) Meleties, M.; Katyal, P.; Lin, B.; Britton, D.; Montclare, J. K. Self-Assembly of Stimuli-Responsive Coiled-Coil Fibrous Hydrogels. *Soft Matter* **2021**, *17* (26), 6470−6476.
(47) Xie, Y.; Upton, Z.; Richards, S.; Rizzi, S. C.; Leavesley, D. I. Hyaluronic Acid: Evaluation as a Potential Delivery Vehicle for Vitronectin: Growth Factor Complexes in Wound Healing Applications. *J. Control. Release Off. J. Control. Release Soc.* **2011**, *153* (3), 225−232.
(48) Haase, I.; Evans, R.; Pofahl, R.; Watt, F. M. Regulation of Keratinocyte Shape, Migration and Wound Epithelialization by IGF-1- and EGF-Dependent Signalling Pathways. *J. Cell Sci.* **2003**, *116* (15), 3227−3238.
(49) Kim, Y. S.; Lee, H.-J.; Han, M.; Yoon, N.; Kim, Y.; Ahn, J. Effective Production of Human Growth Factors in Escherichia Coli by Fusing with Small Protein 6HFh8. *Microb. Cell Factories* **2021**, *20* (1), 9.
(50) Park, S.-R.; Kim, J.-W.; Jun, H.-S.; Roh, J. Y.; Lee, H.-Y.; Hong, I.-S. Stem Cell Secretome and Its Effect on Cellular Mechanisms Relevant to Wound Healing. *Mol. Ther. J. Am. Soc. Gene Ther.* **2018**, *26* (2), 606−617.
(51) Mout, R.; Bretherton, R. C.; Decarreau, J.; Lee, S.; Gregorio, N.; Edman, N. I.; Ahlrichs, M.; Hsia, Y.; Sahtoe, D. D.; Ueda, G.; Sharma, A.; Schulman, R.; DeForest, C. A.; Baker, D. De Novo Design of Modular Protein Hydrogels with Programmable Intra- and Extracellular Viscoelasticity. *Proc. Natl. Acad. Sci. U. S. A.* **2024**, *121* (6), No. e2309457121.

https://doi.org/10.1021/acsbiomaterials.5c00813
ACS Biomater. Sci. Eng. 2025, 11, 4869−4880